

Chemical Reactions-based Detection Mechanism for Molecular Communications

Trang Ngoc Cao*, Vahid Jamali[†], Wayan Wicke[‡], Nikola Zlatanov[§],
Phee Lep Yeoh[¶], Jamie Evans^{||}, and Robert Schober[‡]

Abstract—In molecular communications, the direct detection of signaling molecules may be challenging due to a lack of suitable sensors and interference from co-existing substances in the environment. Motivated by research in molecular biology, we investigate an indirect detection mechanism using chemical reactions between the signaling molecules and a molecular probe to produce an easy-to-measure product at the receiver. We consider two implementations of the proposed detection mechanism, i.e., unrestricted probe movement and probes restricted to a volume around the receiver. In general, the resulting reaction-diffusion equations that describe the concentrations of the reactant and product molecules in the system are non-linear and coupled, and cannot be solved in closed form. To evaluate these molecule concentrations, we develop an efficient iterative algorithm by discretizing the time variable and solving for the space variables of the concentration equations in each time step. The accuracy of our proposed algorithm is verified by particle-based simulations. In the special case when the concentration of the unrestricted probes is high and not changed significantly by the chemical reaction compared to the signaling molecule concentration, we can obtain insightful closed-form solutions. Our results show that the concentrations of the product molecules and the signalling molecules share a similar characteristic over time, i.e., a single peak and a long tail. The peak and tail values of the product molecule concentration can be controlled by choosing probes with suitable parameters, e.g., the diffusion coefficient, reaction rate, and released quantity. We analyze the bit error rate (BER) of the system for a threshold decision rule. Furthermore, we highlight that by carefully choosing the molecular probe and optimizing the decision threshold, the BER can be improved significantly and outperform that of a direct detection system. Moreover, when molecular probes are kept in a small volume around the receiver, fewer resources, i.e., probe molecules, are needed to achieve the same BER and an even higher data rate compared to the case when they are not restricted.

I. INTRODUCTION

In molecular communications (MC), information is typically encoded in the number, type, or time of the release of signaling

This paper was presented in part at the IEEE Wireless Communications and Networking Conference 2020 [1].

T. N. Cao is with the School of Psychological Sciences, Monash University, Melbourne, VIC 3800, Australia (e-mail: trang.cao@monash.edu).

V. Jamali is with the Department of Electrical and Computer, Princeton University, New Jersey 08544, Germany (e-mail: jamali@princeton.edu).

W. Wicke and R. Schober are with the Institute for Digital Communications, Friedrich-Alexander- Universität Erlangen-Nürnberg, Erlangen 91058, Germany (e-mail: wayan.wicke@fau.de; robert.schober@fau.de).

N. Zlatanov is with the Department of Electrical and Computer Systems Engineering, Monash University, Melbourne, VIC 3800, Australia (e-mail: nikola.zlatanov@monash.edu).

P. L. Yeoh is with the School of Electrical and Information Engineering, University of Sydney, Sydney, NSW 2006, Australia (e-mail: phee.yeoh@sydney.edu.au).

J. S. Evans is with the Department of Electrical and Electronic Engineering, University of Melbourne, Melbourne, VIC 3010, Australia (e-mail: jse@unimelb.edu.au).

molecules. The encoded information is detected at the receiver by a sensor [2]–[4]. Therefore, sensor technology, in particular chemical sensors, plays an important role for the design of receivers in MC systems.

Chemical sensors are designed to provide a measurable signal corresponding to the concentration of an analyte (i.e., a chemical substance) in the environment [5]. This measurement can be based on magnetic or electrical fields, resistance, capacitance, inductance, or an optical response [5]. In MC, the selection of the sensor technique depends on the specific requirements of the considered application. For example, magnetic field based sensing was used in [6] and resistance based sensing was applied in [7]. The systems in [6] and [7] have demonstrated the possibility of realizing MC but they are fairly simple since there are no interfering sources impairing the detection of the signaling molecules, i.e., no other magnetic [6] or alcohol sources [7] besides the desired signal. Nevertheless, in many practical applications of MC, e.g., drug delivery and health monitoring, there usually exist other chemical substances which may cause interference for the detection of the signaling molecules. Environmental monitoring applications also need to handle environments where many different chemicals and electromagnetic sources are present and potentially cause interference. For example, chemicals such as zinc and copper have similar magnetic susceptibility and electrical resistivity and thus are difficult to distinguish at the receiver. In such cases, one possible solution for detection is to employ unique chemical reactions where only the signaling molecule, i.e., the analyte, can react with a specific reactant, i.e., a molecular probe, to produce a product molecule which can be easily measured. This approach has been an area of intense research in molecular biology, see [5] and references therein. For example, zinc ions react with spiropyran and produce a merocyanine metal complex, which exhibits fluorescence, i.e., it emits light of a wavelength that can be measured via optical spectroscopy [5], [8]. Furthermore, synthesizing molecular probes that are matched to a given analyte and the considered environment has been an active area of research, see [5] and references therein.

Note that, in some MC systems, the signaling molecules should be small and lightweight, e.g., zinc ions or calcium ions, such that they can be easily stored at the transmitter and can diffuse quickly from the transmitter to the receiver. On the other hand, the product molecules of the reaction, i.e., the combination of the probe and the analyte [9], which can be detected directly by the receiver, are usually larger molecules and thus may not be suitable as quickly-diffusive signaling molecules. Moreover, when the reaction occurs, a measurable

signal, e.g., light, corresponding to the reaction product may be generated but then disappear quickly by a process referred to as quenching [5], [10], [11], which is useful for reducing inter-symbol interference (ISI). Motivated by these advantages, in this work, we propose a novel MC detection mechanism based on the reaction of signaling molecules with a molecular probe.

Chemical reactions have been studied in different contexts for MC. For example, chemical reactions were used to generate signaling molecules at the transmitter [12] and potent drugs on the surface of the receiver [13]. The reactions of signalling molecules with enzymes in the environment were exploited to mitigate ISI in [14], [15]. The reactions of signalling molecules with molecules around the receiver were used for the detection in [13], [16]–[18]. Chemical reactions have also been considered for coding and modulation in [19]–[21]. In [12], the chemical reactions were assumed to occur in a one dimensional environment and the concentration of one reactant was known. The enzyme in [13] and the receptors in [13], [16]–[18], i.e., one of the reactants, were assumed to be immobile. Moreover, the authors in [14], [15] considered a fast reaction where the concentration of the enzymes remained constant. The authors in [19], [20] focused on the concentration of the signaling molecules, i.e., the reactants, but the products of the reaction were of no interest and not studied. In [22], the molecules emitted by the transmitter and the product of the reaction during propagation were both considered, but the reaction was a degradation reaction and thus modeled as a first-order reaction. In [21], approximate solutions of the reaction-diffusion equations are given in the forms of infinite series of functions and recursive equations are used to solve for these functions. However, the approximate solutions is shown to only converge to the true solution if either the simulation time interval or the reaction rate is sufficiently small. Moreover, [21] consider the reaction-diffusion equations for modulation in a two-transmitter system without ISI. In this work, we consider the reaction between signaling molecules and molecular probes, which has to be modeled as a second-order reaction. To the best of the authors' knowledge, second-order reactions with the reactants not being bound to the receiver but diffusing in the environment have not previously been considered for detection design of MC systems with ISI.

We consider two possible implementations of the proposed detection mechanism. We first study the general and simple implementation where the molecular probes are released and then freely diffuse in an unbounded environment. To analyze the system performance, we propose an algorithm to determine the concentration of the product of the detection reaction. We then investigate the special case where the concentration of the molecular probes is high compared to the concentration of the analyte and thus not significantly affected by the chemical reaction. In this case, a closed-form solution for the concentration of the reaction product can be obtained. For the second implementation, instead of distributing the molecular probes everywhere in the environment, we aim for an efficient usage of the probes. To this end, the probes are trapped in a small volume around the receiver. By doing this, the probes can react with the signaling molecules and create more

products to be detected by the receiver instead of dispersing in the environment and being wasted. The probes can be kept inside a volume by a natural or synthetic membrane that only allows the signaling molecules to pass through. In biological systems, a semipermeable natural membrane can block certain types of molecules and allow others to diffuse across it via a process called osmosis [23], [24]. Synthetic membranes can also separate the probes from the external environment via a membrane process, which can be driven by pressure, concentration, or an electric field across the membrane [25]. To analyze the system performance for this implementation, we suitably modify the algorithm developed for freely diffusing probes.

In this paper, we propose a novel MC detection concept based on a chemical reaction between diffusive molecules and make the following main contributions:

- We propose a novel detection mechanism for MC systems in which the direct detection of the signaling molecules is not possible or not efficient. A molecular probe is employed to convert the original signaling molecules into product molecules which can be efficiently detected.
- We develop a robust iterative algorithm for evaluation of the spatio-temporal distribution of the product molecules by solving the underlying non-linear and coupled reaction diffusion equations. We apply the algorithm to two system implementations with suitable adaptations.
- We derive a closed-form expression for the concentration of the product molecules for the case where the concentration of the unrestricted molecular probe is not significantly affected by the chemical reaction.
- We design a system where the probes are restricted to a volume around the receiver to enable an efficient use of the available resources.
- We analyze the performance of the proposed detection mechanism in terms of the bit error rate (BER). Furthermore, we provide new insights for system design with regard to the optimal decision threshold, data rate, efficiency, and the molecular probe's parameters such as the diffusion coefficient, reaction rate, and released quantity.

This paper is an extension of a conference paper [1] which did not consider restricted molecular probe movement and the resulting performance in terms of resource efficiency, BER, and data rate. Moreover, the impact of the system parameters on the product molecule concentration is analyzed more in depth in this paper compared to [1].

The remainder of this paper is organized as follows. In Section II, we introduce the system model and the proposed detection mechanism. In Section III, we analyze the molecule concentrations for three implementations of the proposed detection mechanism and the resulting detection performance. Numerical results are presented in Section IV, and Section V concludes the paper.

II. SYSTEM MODEL AND DETECTION MECHANISM

We consider an MC system consisting of a point source transmitter, denoted by Tx, and a transparent receiver, denoted

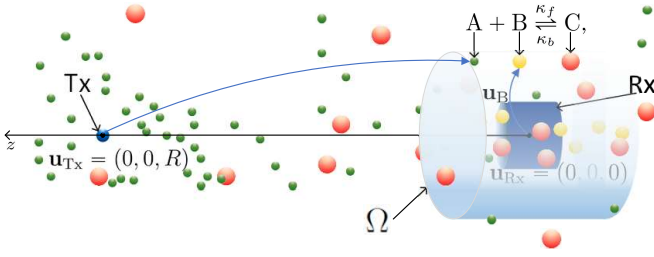


Fig. 1. Schematic illustration of the system model. Type A molecules are released from the transmitter, Tx, and react with type B molecules, released at position \mathbf{u}_B , in order to create type C molecules, which can be measured by the receiver, Rx. The B molecules can be restricted in volume Ω around Rx.

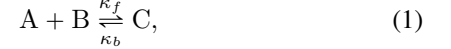
by Rx, in an unbounded three dimensional (3D) diffusive environment with constant temperature and viscosity. The receiver has volume \mathcal{V}_{Rx} and is located at distance R from the transmitter. Using cylindrical coordinates¹, where position \mathbf{u} is defined as $\mathbf{u} = (\rho, \phi, z)$, $\rho \in [0, \infty)$, $\phi \in [0, 2\pi)$, and $z \in (-\infty, \infty)$, Tx and Rx are centered at $\mathbf{u}_{Tx} = (0, 0, R)$ and $\mathbf{u}_{Rx} = (0, 0, 0)$, respectively. Let T denote the duration of a symbol interval. We assume on-off keying modulation and that Tx releases N_A molecules of type A to convey bit “1” and no molecules to convey bit “0” at the beginning of the symbol interval, i.e., at $t = nT$, $n = 0, 1, \dots, N$, where N is the length of the bit sequence. We assume that bits “0” and “1” have equal probabilities.

We assume that the type A molecules cannot be detected directly at the receiver as a suitable sensor is not available. Hence, type B molecules are introduced into the system to react with the type A molecules to create type C molecules for which suitable sensors are available, see Fig. 1. The type B molecules are referred to as molecular probes [26]. The type B molecules may be released at a fixed position, denoted by \mathbf{u}_B , e.g., $\mathbf{u}_B = \mathbf{u}_{Rx}$, or uniformly throughout the environment. Furthermore, the type B molecules may be restricted to a volume around the receiver, denoted by Ω . In cylindrical coordinates, we assume Ω to be the cylindrical volume bounded by $0 \leq \rho \leq a$, $0 \leq \phi < 2\pi$, and $-\frac{b}{2} \leq z \leq \frac{b}{2}$.² When type B molecules diffuse freely in an unbounded environment, we have $a, b \rightarrow \infty$. We model the sensing process via a transparent receiver which counts the number of the type C molecules in its volume without affecting the molecules. For example, for the detection of the

¹We choose cylindrical coordinates so that calculations for the symmetric systems can be simplified.

²Cylinder, i.e., rod shape, is a common morphology of cells and bacteria, which was optimized by evolution [27], [28]. Since MC is provisioned to be applied in biological systems such as human bodies, cylinder is a good choice for MC system designs in order to leverage the advantages of this morphology.

zinc ions mentioned in the introduction, optical spectroscopy is used to measure the light intensity which is proportional to the number of product molecules, i.e., the type C molecules. We note that the effect of quenching, which could be exploited for ISI reduction, is neglected and left for future work. We assume that the chemical reaction between the type A and B molecules is reversible and can be modeled as follows



where κ_f is the forward reaction rate constant of a second-order reaction and κ_b is the backward reaction rate constant of a first-order reaction. We assume that the type A, B, and C molecules diffuse in the unbounded 3D environment with diffusion coefficients D_A , D_B , and D_C , respectively. Thereby, the concentrations of the type A, B, and C molecules at time t and position \mathbf{u} , denoted by $C_i(\mathbf{u}, t)$, $i \in \{A, B, C\}$, are governed by a set of reaction diffusion equations in (2) [29, Eqs. (9.5), (9.13)], given at the bottom of this page, where ∇^2 is the Laplace operator and

$$G_i(\mathbf{u}, t) = \sum_{t_i} \sum_{\mathbf{u}_i} N_i \delta_d(t - t_i) \delta_d(\mathbf{u} - \mathbf{u}_i), \quad i \in \{A, B\}, \quad (3)$$

represents the concentration of the type i molecules that are released into the channel. In (3), $\delta_d(\cdot)$, N_i , t_i , and \mathbf{u}_i are the Dirac delta function, the number of molecules released at time t_i , the release times, and the release positions of the type i molecules, respectively. The partial differential equations (PDEs) in (2) are non-linear and coupled, i.e., the concentration of the type i molecules after n releases is not equal to the sum of the concentrations originating from each release. Thus, the PDEs in (2) do not have a closed-form solution in general [14], [20], [30]. On the other hand, we need to obtain $C_C(\mathbf{u}, t)$ to design the proposed MC system and to analyze its performance. To this end, in the next section, we will propose an algorithm for solving (2) for $C_C(\mathbf{u}, t)$ and analyze the system performance.

III. SYSTEM ANALYSIS FRAMEWORK

In this section, we consider two implementations of the proposed detection mechanism. We first start with an implementation of the detector when the location of the probes is not restricted. We then consider the special case where the concentration of the unrestricted probes is constant over time. Second, we investigate an implementation of the detector with probes restricted in a small volume around the receiver. We present an efficient numerical algorithm for determining $C_i(\mathbf{u}, t)$, $i \in \{A, B, C\}$, which can be used for both implementations. For the special case of unrestricted probes of constant concentration, we derive analytical expressions for $C_i(\mathbf{u}, t)$.

$$\frac{\partial C_A(\mathbf{u}, t)}{\partial t} = G_A(\mathbf{u}, t) + D_A \nabla^2 C_A(\mathbf{u}, t) - \kappa_f C_A(\mathbf{u}, t) C_B(\mathbf{u}, t) + \kappa_b C_C(\mathbf{u}, t), \quad (2a)$$

$$\frac{\partial C_B(\mathbf{u}, t)}{\partial t} = G_B(\mathbf{u}, t) + D_B \nabla^2 C_B(\mathbf{u}, t) - \kappa_f C_A(\mathbf{u}, t) C_B(\mathbf{u}, t) + \kappa_b C_C(\mathbf{u}, t), \quad (2b)$$

$$\frac{\partial C_C(\mathbf{u}, t)}{\partial t} = D_C \nabla^2 C_C(\mathbf{u}, t) + \kappa_f C_A(\mathbf{u}, t) C_B(\mathbf{u}, t) - \kappa_b C_C(\mathbf{u}, t), \quad (2c)$$

Algorithm 1 Iterative Calculation of the Concentrations

Initialization: $t = 0, \Delta t, T^{\max}$, and $C_i(\mathbf{u}, t = 0)$.

while $t \leq T^{\max}$ **do**

 Update t as $t + \Delta t$.

 Compute $\bar{G}_i(\mathbf{u})$ by (5), $C_i^{\text{df}}(\mathbf{u}, t)$ by (6), and $C_i^{\text{rc}}(\mathbf{u}, t)$ by (9), concurrently for all i .

 Update $C_i(\mathbf{u}, t)$ based on (4), concurrently for all i .

end while

Return $C_i(\mathbf{u}, t)$.

Finally, we analyze the performance of the system for a simple decision rule.

A. Detection with Unrestricted Probes

In this subsection, we consider the detection in an unbounded environment, i.e., bounds $a, b \rightarrow \infty$ in cylindrical coordinates. For determining $C_i(\mathbf{u}, t)$, we adapt [20, Algorithm 1] to the problem at hand. The basic concept behind this algorithm is to discretize the time variable and solve the PDEs in terms of the space variable. Considering small time intervals allows us to decouple the diffusion and reaction equations³. In particular, Algorithm 1, shown at the top of the page, summarizes the steps needed for calculating the concentrations of the type A, B, and C molecules, where T^{\max} is the maximum time considered. We will verify the accuracy of the resulting numerical algorithm via particle-based simulation in Section IV.

In Algorithm 1, $C_i(\mathbf{u}, t)$ is updated for $i = \{A, B, C\}$ in each iteration as follows [20]

$$C_i(\mathbf{u}, t + \Delta t) = \bar{G}_i(\mathbf{u}) + C_i^{\text{df}}(\mathbf{u}, t + \Delta t) + C_i^{\text{rc}}(\mathbf{u}, t + \Delta t) - C_i(\mathbf{u}, t), \quad (4)$$

where $\bar{G}_i(\mathbf{u})$ is the concentration of the type i molecules released at \mathbf{u} in time interval $[t, t + \Delta t]$. $C_i^{\text{df}}(\mathbf{u}, t + \Delta t)$ and $C_i^{\text{rc}}(\mathbf{u}, t + \Delta t)$ are the concentrations of the type i molecules assuming that in interval $[t, t + \Delta t]$ only diffusion and only reactions occur, respectively, while the other phenomenon is absent. The updates of the concentrations in (4) are given in the following.

1) *Update of Release:* As proved in [20], $\bar{G}_i(\mathbf{u})$ is given by

$$\bar{G}_i(\mathbf{u}) = \sum_{t_i} N_i \delta_d(t + \Delta t - \varepsilon - t_i) \delta_d(\mathbf{u}), \quad (5)$$

³For a detailed mathematical proof of the accuracy of the algorithm with respect to the decoupling of diffusion and reaction, please refer to [20].

where ε is an arbitrary small positive real number satisfying $\varepsilon \ll \Delta t$ and t_i is given by $t_i = m\Delta t - \varepsilon, m \in \mathbb{N}$.

2) *Update of $C_i^{\text{df}}(\mathbf{u}, t + \Delta t)$:* As shown in [20],

$$C_i^{\text{df}}(\mathbf{u}, t + \Delta t) = \frac{1}{(4\pi D_i \Delta t)^{3/2}} \int_{\tilde{\mathbf{u}}} C_i(\tilde{\mathbf{u}}, t) \times \exp\left(-\frac{\|\mathbf{u} - \tilde{\mathbf{u}}\|^2}{4D_i \Delta t}\right) d\tilde{\mathbf{u}}. \quad (6)$$

Due to the symmetry of the system, we choose cylinder coordinates to simplify the calculation of (6) in Corollary 1.

Corollary 1: Using cylindrical coordinates, $C_i^{\text{df}}(\mathbf{u}, t + \Delta t)$ is given by

$$C_i^{\text{df}}(\mathbf{u}, t + \Delta t) = \frac{2\pi}{(4\pi D_i \Delta t)^{3/2}} \int_{\tilde{\rho}=0}^{\infty} \int_{\tilde{z}=-\infty}^{\infty} C_i(\tilde{\rho}, \tilde{z}, t) \times W_i^z(z, \tilde{z}) W_i^{\rho}(\rho, \tilde{\rho}) d\tilde{z} d\tilde{\rho}, \quad (7)$$

where

$$W_i^z(z, \tilde{z}) = \exp\left(-\frac{(z - \tilde{z})^2}{4D_i \Delta t}\right), \quad (8a)$$

$$W_i^{\rho}(\rho, \tilde{\rho}) = \exp\left(-\frac{\rho^2 - \tilde{\rho}^2}{4D_i \Delta t}\right) \tilde{\rho} I_0\left(\frac{\rho \tilde{\rho}}{2D_i \Delta t}\right), \quad (8b)$$

and $I_0(\cdot)$ is the zeroth order modified Bessel function of the first kind.

Proof: Please refer to Appendix A. \square

Note that $W_i^z(z, \tilde{z})$ and $W_i^{\rho}(\rho, \tilde{\rho})$ do not change over time, and thus, can be evaluated offline and used online in order to reduce computational complexity.

3) *Update of $C_i^{\text{rc}}(\mathbf{u}, t)$:* Since, in this work, the product of the reaction is used for detection whereas in [20] it was of no interest for the considered system, the reaction diffusion equations in [20] are different from those in this work. Hence, in order to use Algorithm 1, we require $C_i^{\text{rc}}(\mathbf{u}, t)$, which is given in the following theorem.

Theorem 1: The concentration of the type $i \in \{A, B, C\}$ molecules at time t and position \mathbf{u} assuming that only reactions occur and diffusion is absent is given by (9) at the bottom of this page, where

$$c_{11}(\mathbf{u}) = C_A(\mathbf{u}, t) - C_B(\mathbf{u}, t), \quad (10)$$

$$c_{12}(\mathbf{u}) = C_A(\mathbf{u}, t) + C_C(\mathbf{u}, t), \quad (11)$$

$$c_2(\mathbf{u}) = \sqrt{(-\kappa_f c_{11}(\mathbf{u}) + \kappa_b)^2 + 4\kappa_f \kappa_b c_{12}(\mathbf{u})}, \quad (12)$$

$$c_3(\mathbf{u}) = C_A(\mathbf{u}, t) + C_B(\mathbf{u}, t), \quad (13)$$

$$c_4(\mathbf{u}) = \frac{c_2(\mathbf{u}) - \kappa_f c_3(\mathbf{u}) - \kappa_b}{c_2(\mathbf{u}) + \kappa_f c_3(\mathbf{u}) + \kappa_b}. \quad (14)$$

$$C_A^{\text{rc}}(\mathbf{u}, t + \Delta t) = \frac{c_2(\mathbf{u}) + \kappa_f c_{11}(\mathbf{u}) - \kappa_b - (c_2(\mathbf{u}) - \kappa_f c_{11}(\mathbf{u}) + \kappa_b) c_4(\mathbf{u}) \exp(-c_2(\mathbf{u})\Delta t)}{2\kappa_f (1 + c_4(\mathbf{u}) \exp(-c_2(\mathbf{u})\Delta t))}, \quad (9a)$$

$$C_B^{\text{rc}}(\mathbf{u}, t + \Delta t) = \frac{c_2(\mathbf{u}) - \kappa_f c_{11}(\mathbf{u}) - \kappa_b - (c_2(\mathbf{u}) + \kappa_f c_{11}(\mathbf{u}) + \kappa_b) c_4(\mathbf{u}) \exp(-c_2(\mathbf{u})\Delta t)}{2\kappa_f (1 + c_4(\mathbf{u}) \exp(-c_2(\mathbf{u})\Delta t))}, \quad (9b)$$

$$C_C^{\text{rc}}(\mathbf{u}, t + \Delta t) = c_{12}(\mathbf{u}) - C_A^{\text{rc}}(\mathbf{u}, t + \Delta t), \quad (9c)$$

Proof: Please refer to Appendix B. \square

In some applications, the backward reaction can be very slow with respect to the time scale of interest. When $\kappa_b \rightarrow 0$ and $C_A(\mathbf{u}, t) = C_B(\mathbf{u}, t)$ hold, (9a) and (9b) have indeterminate forms. For this case, the values of $C_i^{\text{rc}}(\mathbf{u}, t + \Delta t)$ are given in the following corollary.

Corollary 2: For $\kappa_b = 0$ and $C_A(\mathbf{u}, t = 0) = C_B(\mathbf{u}, t = 0)$, we have

$$C_A^{\text{rc}}(\mathbf{u}, t + \Delta t) = C_B^{\text{rc}}(\mathbf{u}, t + \Delta t) = \frac{C_A(\mathbf{u}, t)}{1 + \kappa_f \Delta t C_A(\mathbf{u}, t)} \quad (15)$$

and $C_C^{\text{rc}}(\mathbf{u}, t + \Delta t)$ is still given by (9c).

Proof: When $\kappa_b \rightarrow 0$ and $C_A(\mathbf{u}, t) = C_B(\mathbf{u}, t)$, (15) is obtained by using L'Hospital's rule in (9a) and (9b) for $c_{11}(\mathbf{u}) \rightarrow 0$. \square

B. Detection with Unrestricted and Steady-Concentration Probes

In this subsection, we consider the special case when $C_B(\mathbf{u}, t)$ is very large and thus is not changed significantly by the reaction over time, i.e., $C_B(\mathbf{u}, t)$ is assumed to be constant over time. This assumption is similar to the assumption of constant enzyme concentration made in [14]. The assumption is applicable when the type B molecules have been released continuously over time from a position \mathbf{u}_B such that a steady state is reached at the beginning of information transmission. The steady state value of $C_B(\mathbf{u}, t)$ is given by

$$\begin{aligned} C_B(\mathbf{u}) &= \lim_{t \rightarrow \infty} \int_0^t C_B(\mathbf{u}, \tilde{t}) d\tilde{t} \\ &= \lim_{t \rightarrow \infty} \frac{N_B}{4\pi D_B t} \operatorname{erfc} \left(\frac{\|\mathbf{u} - \mathbf{u}_B\|}{\sqrt{4D_B t}} \right) \\ &= \frac{N_B}{4\pi D_B \|\mathbf{u} - \mathbf{u}_B\|}, \end{aligned} \quad (16)$$

where $\operatorname{erfc}(\cdot)$ is the complementary error function. Then, if $\kappa_b = 0$, and $D_A = D_C$, we can obtain closed-form expressions for $C_A(\mathbf{u}, t)$ and $C_C(\mathbf{u}, t)$, as given in the following corollary.

Corollary 3: Under the above assumption, the concentrations of the type A and C molecules are given respectively by

$$C_A(\mathbf{u}, t) = \frac{N_A}{(4\pi D_A t)^{3/2}} \exp \left(-\frac{\|\mathbf{u} - \mathbf{u}_A\|^2}{4D_A t} - \kappa_f C_B(\mathbf{u}, t) \right), \quad (17)$$

$$C_C(\mathbf{u}, t) = \frac{N_A}{(4\pi D_A t)^{3/2}} \exp \left(-\frac{\|\mathbf{u} - \mathbf{u}_A\|^2}{4D_A t} \right) - C_A(\mathbf{u}, t), \quad (18)$$

where \mathbf{u}_A is the release position of the type A molecules.

Proof: Please refer to Appendix C. \square

Remark 1: Due to (2c), $C_C(\mathbf{u}, t)$ in (18) increases rapidly when $C_B(\mathbf{u}, t)$ is large. For the general case, where $C_B(\mathbf{u}, t)$ reduces over time, $C_C(\mathbf{u}, t)$ given in (18) is an upper bound.

C. Detection with Restricted Probes

To use the probe molecules efficiently, we consider an MC system where the molecular probes, i.e., type B molecules, are restricted to volume Ω around the receiver. Hence, the type B molecules will not disperse in the environment and more type C molecules are produced around the receiver. Note that, type A and C molecules can diffuse in an unbounded environment. In this case, the concentration of type A, B, and C molecules can still be calculated with Algorithm 1 except that $C_B(\mathbf{u}, t) = 0$, $\mathbf{u} \notin \Omega$, and $C_B^{\text{df}}(\mathbf{u}, t)$, $\mathbf{u} \in \Omega$, is updated as specified in the following Corollary.

Corollary 4: Using cylindrical coordinates, for a bounded volume, $C_B^{\text{df}}(\mathbf{u}, t + \Delta t)$, $\mathbf{u} \in \Omega$, is given by

$$\begin{aligned} C_B^{\text{df}}(\mathbf{u}, t + \Delta t) &= \frac{4}{a^2 b} \int_{\tilde{\rho}=0}^a \int_{\tilde{z}=-\frac{b}{2}}^{\frac{b}{2}} C_B(\tilde{\rho}, \tilde{z}, t) W_B^z(z, \tilde{z}) \\ &\quad \times W_B^\rho(\rho, \tilde{\rho}) d\tilde{z} d\tilde{\rho}, \end{aligned} \quad (19)$$

where $W_B^z(z, \tilde{z})$ and $W_B^\rho(\rho, \tilde{\rho})$ are given by (20) at the bottom of this page, $J_0(\cdot)$ is the zeroth order Bessel function of the first kind, and l_j is the positive root of $J'_0(l_j) = 0$.

Proof: Please refer to Appendix D. \square

Note that, for a given amount of released type B molecules, the smaller volume Ω is, the higher the concentration of the type B molecules in the volume Ω is. For a small volume Ω , a slight increase in the released number of type B molecules can result in a large increase in the concentration of the type B molecules in the volume. This leads to a large increase in the concentration of the created type C molecules.

D. Threshold Decision Rule

Let s_n and \hat{s}_n ($s_n, \hat{s}_n \in \{0, 1\}$) denote the n -th transmitted bit and the n -th detected bit, respectively. We adopt a simple threshold decision rule at the receiver where the receiver makes the decision on the transmitted bit based on a signal which is proportional to the number of type C molecules in its volume, denoted by q , at the sampling time, denoted by t_s , as follows

$$\hat{s}_n = \begin{cases} 0 & \text{if } q \leq \gamma, \\ 1 & \text{if } q > \gamma, \end{cases} \quad (21)$$

where γ is the decision threshold. We assume that the movements of the molecules are mutually independent, and thus, q approximately follows a Poisson distribution [2] as follows

$$q \sim \mathcal{P}(\bar{q}), \quad (22)$$

$$W_B^z(z, \tilde{z}) = \frac{1}{2} + \sum_{n=1}^{\infty} \cos \left(\frac{n\pi z}{b} \right) \cos \left(\frac{n\pi \tilde{z}}{b} \right) \exp \left(-\frac{n^2 \pi^2}{b^2} D \Delta t \right), \quad (20a)$$

$$W_B^\rho(\rho, \tilde{\rho}) = \tilde{\rho} \left(1 + \sum_{j=1}^{\infty} \frac{1}{J_0^2(l_j)} J_0 \left(\frac{l_j}{a} \rho \right) J_0 \left(\frac{l_j}{a} \tilde{\rho} \right) \exp \left(-\frac{l_j^2}{a^2} D \Delta t \right) \right), \quad (20b)$$

TABLE I
SYSTEM PARAMETERS USED FOR THE NUMERICAL RESULTS.

Parameter	Value	Parameter	Value
D_A [m ² /s]	10×10^{-10}	κ_f [molecules ⁻¹ · m ³ · s ⁻¹]	10^{-22}
D_B [m ² /s]	1.1×10^{-10}	κ_b [s ⁻¹]	10^{-26}
D_C [m ² /s]	10^{-10}	$b = 2a$ [m]	10^{-5}
Δt [s]	10^{-2}	T [s]	10
V_{R_x} [m ³]	9.8×10^{-20}	R [m]	5×10^{-5}
N_A [molecules]	5×10^8	z_{\max} [m]	$6R = 3 \times 10^{-4}$
\mathbf{u}_{T_x} [m]	(0, 0, R)	\mathbf{u}_{R_x} [m]	(0, 0, 0)

where \bar{q} is the mean of q and given by [31]

$$\bar{q} = \int_{\mathbf{u} \in \mathcal{V}_{R_x}} C_C(\mathbf{u}, t_s) d\mathbf{u}. \quad (23)$$

Note that since (2) includes the impact of all releases, $C_C(\mathbf{u}, t_s)$ and thus \bar{q} is affected by ISI and have different values for different sequences of n bits, denoted by $\mathbf{s}_n = [s_1, s_2, \dots, s_n]$.

The BER is given by

$$P_b = \frac{1}{2} \left(\Pr(q \leq \gamma | s_n = 1) + 1 - \Pr(q \leq \gamma | s_n = 0) \right), \quad (24)$$

where the cumulative distribution function of the Poisson distribution can be expressed as

$$\Pr(q \leq \gamma | s_n) = \frac{1}{2^{n-1}} \sum_{\mathbf{s}_{n-1} \in \mathbb{S}} \left(\exp(-\bar{q}) \sum_{w=0}^{\gamma} \frac{\bar{q}^w}{w!} \right). \quad (25)$$

Here, \mathbb{S} is the set of all possible values of \mathbf{s}_{n-1} which affect \bar{q} .

IV. SIMULATION RESULTS

In this section, we first confirm the accuracy of Algorithm 1 by particle-based simulation. We then use Algorithm 1 to analyze the concentration of the type C molecules for different scenarios. We also evaluate the system performance in terms of the BER and use Monte-Carlo simulation to confirm the analytical results.

We simulate the system in a bounded environment using cylindrical coordinates with the limits for ρ and z large enough to approximate an unbounded environment. Let z_{\max} characterize the boundary of the environment such that $0 \leq \rho \leq z_{\max}$, $-z_{\max} \leq z \leq z_{\max}$. For all numerical results presented, we use the parameters provided in Table I, unless otherwise stated. For fast detection, we consider fast forward reactions, e.g., reactions with half-life time on the order of minutes or seconds. The half-life time of a reaction, denoted by $t_{1/2}$, is defined as the time for the concentration of the reactant to decrease to half of its original value [29], assuming the reactant is uniformly distributed. To select suitable parameter orders, we consider the case when the reactants are uniformly distributed and assume that the most significant change of concentration results from the forward reaction in (1), $t_{1/2} = 1$ s, and $C_A(\mathbf{u}, t) \ll C_B(\mathbf{u}, t)$, so that the type A molecules can react and be converted to type C molecules without a noticeable

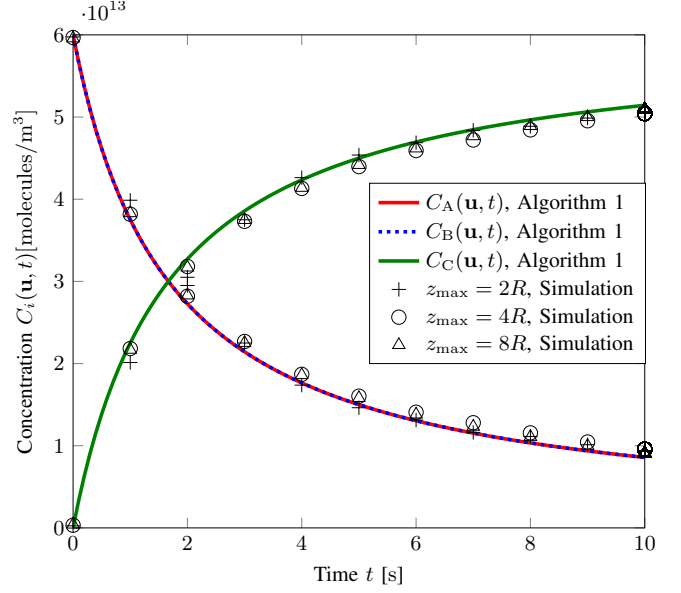


Fig. 2. Concentrations of the type A, B, and C molecules versus time, where the type A and B molecules are uniformly distributed in an approximately-unbounded environment limited by z_{\max} .

reduction of the number of type B molecules. Then, from [29, Eq. (9.14)], we have

$$\kappa_f t_{1/2} = \frac{1}{C_B^0} \ln \left(\frac{C_B^0 - \frac{1}{2} C_A^0}{\frac{1}{2} C_A^0 C_B^0} C_A^0 \right) \simeq \frac{\ln 2}{C_B^0}, \quad (26)$$

where $C_i^0 = C_i(\mathbf{u}, t = 0)$. Adopting $C_B^0 = 6 \times 10^{21}$ molecules/m³ and binding constant $K_a = \kappa_f / \kappa_b = 6 \times 10^4$ molecules⁻¹ · m³ from [9], based on (26), we chose κ_f and κ_b as in Table I such that the resulting K_a is on the same order as K_a in [9].

A. Verification of the Proposed Algorithm and Poisson Model

In Fig. 2, we use the particle-based simulation described in [20, Appendix F] to confirm the accuracy of Algorithm 1, i.e., the solution of the reaction diffusion equation (2). We assume that the type A, B, and C molecules are uniformly distributed with $C_A(\mathbf{u}, t = 0) = C_B(\mathbf{u}, t = 0) = 6 \times 10^{13}$ molecules/m³, and $C_C(\mathbf{u}, t = 0) = 0$ molecules/m³, and they have the same diffusion coefficient D_A given in Table I such that diffusion does not have any impact on the concentrations of the type

A, B, and C molecules⁴. In order to reduce the computational complexity for particle-based simulation, we choose $\kappa_f = 10^{-14} \text{ molecules}^{-1} \cdot \text{m}^3 \cdot \text{s}^{-1}$ and $\kappa_b = 10^{-18} \text{ s}^{-1}$. In Fig. 2, since the value of κ_f is larger than that of κ_b and $C_A(\mathbf{u}, t = 0) = C_B(\mathbf{u}, t = 0)$, we observe that $C_A(\mathbf{u}, t)$ and $C_B(\mathbf{u}, t)$ are equal and decrease over time while $C_C(\mathbf{u}, t)$ increases over time as expected. In general, the results obtained with Algorithm 1 are in good agreement with the simulation results. The simulation results become more accurate for larger z_{\max} , when the assumption of an unbounded environment becomes more justified.

In Fig. 3, we use particle-based simulation to confirm the accuracy of Corollary 3, i.e., the solution of the diffusion equation in a bounded environment. We simulate the diffusion of the type B molecules with $N_B = 10^8$ molecules and adopt $b = 2a = 10^{-5} \text{ m}$. We compare the concentrations of the type B molecules at the release point $\mathbf{u} = \mathbf{u}_B = (0, 0, 0)$, half way to the boundary $\mathbf{u} = (0, 0, b/4)$, and at the boundary $\mathbf{u} = (0, 0, b/2)$. Due to the bounded environment, the concentration of the type B molecules reaches a steady state, i.e., a constant value everywhere in the environment, after a period of time. As expected, at the release point $\mathbf{u} = (0, 0, 0)$, C_B decreases from the highest value at the time of release to the steady value. At the half way point to the boundary $\mathbf{u} = (0, 0, b/4)$, C_B first increases from zero to a maximum, and then decreases to the steady value. At the boundary $\mathbf{u} = (0, 0, b/2)$, C_B increases from zero to the steady value. We also show C_B at the release point for an unbounded environments. The two curves for C_B at the release point for the bounded and unbounded environments are identical for small t . However, C_B for the unbounded environment decreases to zero for large t . In general, the results obtained by Corollary 3 are in excellent agreement with the simulation results.

In Fig. 4, we use particle-based simulation to validate the assumption that the number q of type C molecules in the receiver volume is Poisson distributed, see (22). We use the same simulation setup as for Fig. 2 to obtain the histogram for q , i.e., an estimate for the true distribution. We compare this result with the probability mass function (PMF) of the Poisson distribution with the mean given in (23), $C_C(\mathbf{u}, t)$ obtained by using Algorithm 1, and a receiver volume \mathcal{V}^{Rx} equal to $5.24 \times 10^{-13} \text{ m}^3$. In particular, in Fig. 4, we show the PMF of q observed at times $t_s = [1, 2, 3] \text{ s}$. The corresponding mean values used for the PMF are 11.8, 17.1, and 20.2, respectively, which are obtained from $C_C(\mathbf{u}, t)$ shown in Fig. 2. We observe that the Poisson distributions with the mean obtained with Algorithm 1 are in good agreement with the histograms obtained by particle-based simulation. Thus, the assumption of the Poisson model for the type C product molecules is justified.

B. Impact of System Parameters on Concentration of Type C Molecules

In Fig. 5, we present the concentrations of the type A and C molecules at the center of the receiver versus time for direct

⁴If $D_A > D_B$, for example, after a reaction occurred at a location, type A molecules may diffuse to that location faster than type B molecules and the concentrations of type A and B molecules at that location can be different.

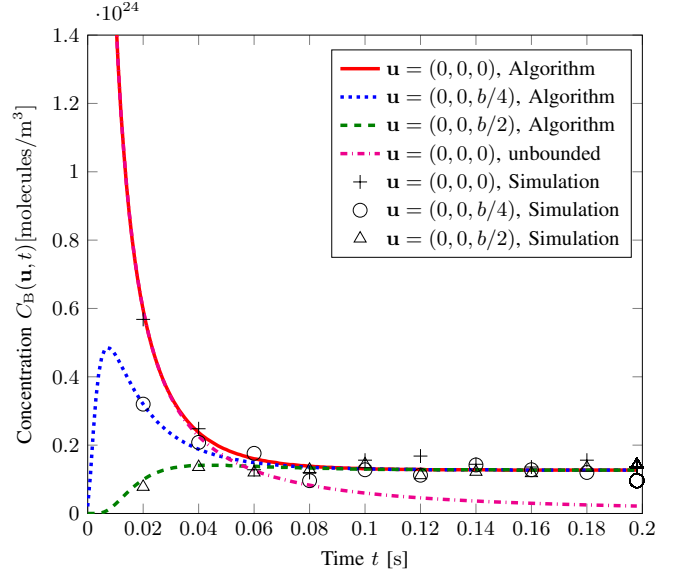


Fig. 3. Concentrations of type B molecules at different positions in unbounded and bounded volumes.

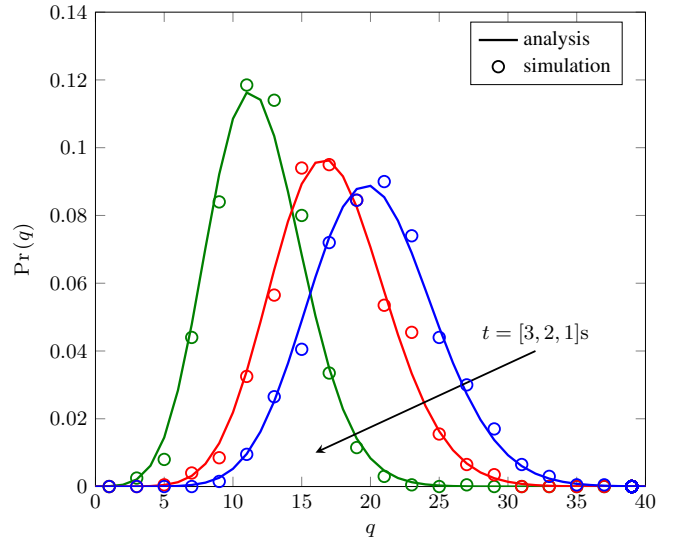


Fig. 4. PMFs of the number q of type C molecules in receiver volume $\mathcal{V}^{\text{Rx}} = 5.24 \times 10^{-13} \text{ m}^3$ at three sample times $t_s = [1, 2, 3] \text{ s}$.

and indirect detection, respectively, when the type B molecules are not restricted. For the proposed indirect detection, we study the impact of the diffusion coefficient and the number of type B molecules released at the center of the receiver on the concentration of the type C molecules. In particular, we assume $\mathbf{u}_B = \mathbf{u}_{\text{Rx}}$, $D_B = [1.1, 5] \times 10^{-10} \text{ m}^2/\text{s}$, and $N_B = [2.4, 24] \times 10^9$ molecules. We observe that when the type A molecules cannot be detected directly, and thus, the proposed indirect detection is used, the concentration of the type C molecules at the center of the receiver, $C_C(\mathbf{u}_{\text{Rx}}, t)$, has a similar characteristic, i.e., a single peak and a long tail, as $C_A(\mathbf{u}_{\text{Rx}}, t)$ when the type A molecules can be directly detected. Let $\max_t C_i(\mathbf{u}_{\text{Rx}}, t)$, $i \in \{A, C\}$, denote the peak value of $C_i(\mathbf{u}_{\text{Rx}}, t)$, i.e., the maximum value of $C_i(\mathbf{u}_{\text{Rx}}, t)$ over time. For larger N_B and a given D_B , e.g., $D_B =$

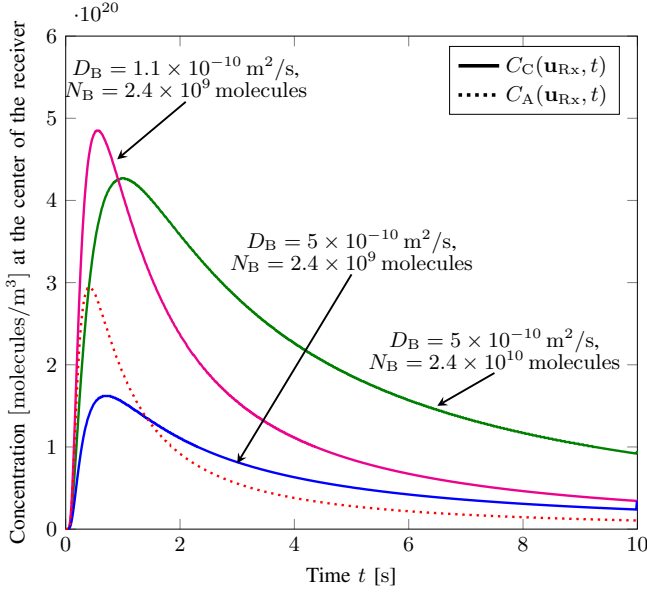


Fig. 5. Concentration of type A and C molecules at the center of the receiver versus time for direct and indirect detection, respectively, when the type B molecules are not restricted. For the latter case, different values of D_B and N_B are considered.

$5 \times 10^{-10} \text{ m}^2/\text{s}$, $\max_t C_C(\mathbf{u}_{Rx}, t)$ is larger. This is expected since a larger number of type B molecules produce a larger number of type C molecules at the receiver. $\max_t C_C(\mathbf{u}_{Rx}, t)$ can even exceed $\max_t C_A(\mathbf{u}_{Rx}, t)$ because $D_C < D_A$ and type C molecules diffuse away from the receiver more slowly than type A molecules. However, the tail of $C_C(\mathbf{u}_{Rx}, t)$ can be heavier than that of $C_A(\mathbf{u}_{Rx}, t)$. In particular, for $N_B = 2.4 \times 10^9$ molecules, although $\max_t C_C(\mathbf{u}_{Rx}, t) < \max_t C_A(\mathbf{u}_{Rx}, t)$, the tail of $C_C(\mathbf{u}_{Rx}, t)$ is heavier than that of $C_A(\mathbf{u}_{Rx}, t)$ for the considered range of time t . This may negatively affect system performance due to the increased level of ISI as will be shown in Fig. 9. Nevertheless, using the type C molecules for detection is unavoidable when direct detection of the type A molecules is *impossible*. Moreover, for a given N_B , e.g., $N_B = 2.4 \times 10^9$ molecules, and smaller D_B , e.g., $D_B = 1.1 \times 10^{-10} \text{ m}^2/\text{s}$, $\max_t C_C(\mathbf{u}_{Rx}, t)$ is also larger. Smaller D_B result in slower diffusion of type B molecules from the receiver. Thus, there are more type B molecules near the receiver to react and produce more type C molecules. However, due to the larger number of reactions, the amount of the type B molecules in the environment reduces significantly and thus less type C molecules are produced at later times, which results in a lighter tail of $C_C(\mathbf{u}_{Rx}, t)$, i.e., less ISI.

In Fig. 6, we investigate the impact of k_f and N_B on $C_C(\mathbf{u}_{Rx}, t)$ when the type B molecules are not restricted. In particular, we present the concentrations of the type A and C molecules at the center of the receiver versus time for direct detection and indirect detection with $k_b = 0$, $D_A = D_B = D_C = 1 \times 10^{-9} \text{ m}^2/\text{s}$. We consider $N_B = 2.4 \times 10^9$ molecules and $k_f = [100, 10, 5, 1] \times 10^{-22} \text{ molecules}^{-1} \cdot \text{m}^3 \cdot \text{s}^{-1}$ as well as $N_B = 2 \times 10^8$ molecules and $k_f = 10^{-18} \text{ molecules}^{-1} \cdot \text{m}^3 \cdot \text{s}^{-1}$. We observe that the concentration of the type C molecules in-

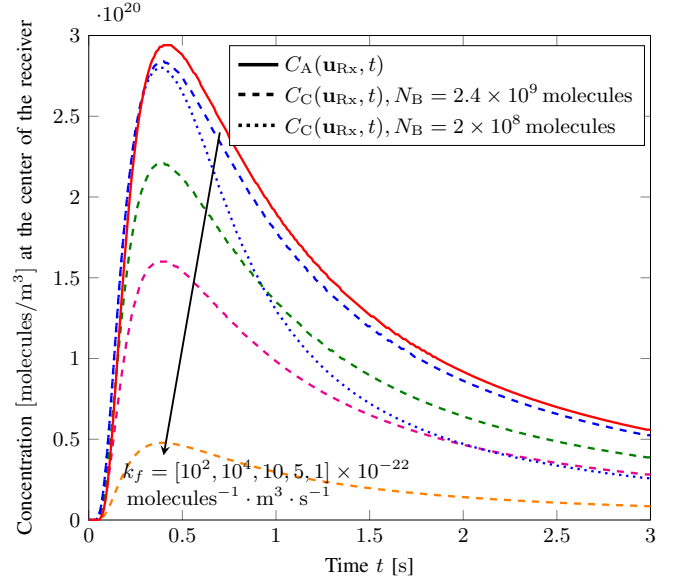


Fig. 6. Concentration of type A and C molecules at the center of the receiver versus time for direct and indirect detection, respectively, when the type B molecules are not restricted.

creases quickly after the release of the type A and B molecules and the peak value of the concentration increases when k_f increases. This means more type C molecules are created when the reaction rate is larger. The concentration of the type C molecules approaches the concentration of the type A molecules for large k_f . For $N_B = 2.4 \times 10^9$ molecules and $k_f = 10^{-20} \text{ molecules}^{-1} \cdot \text{m}^3 \cdot \text{s}^{-1}$, $C_C(\mathbf{u}_{Rx}, t) \approx C_A(\mathbf{u}_{Rx}, t)$. This means k_f is large enough such that the reaction between type A and B molecules happens immediately whenever they come close to each other. Thus, most of the type A molecules will become type C molecules. Increasing k_f further would not result in any significant change of $C_C(\mathbf{u}_{Rx}, t)$. Note that the immediate reaction alone is not enough to yield $C_C(\mathbf{u}_{Rx}, t) \approx C_A(\mathbf{u}_{Rx}, t)$ as $D_A = D_C$ is also needed for the created type C molecules to diffuse in the same manner as the type A molecules. For a smaller N_B , e.g., $N_B = 2 \times 10^8$ molecules, and sufficiently large k_f , e.g., $k_f = 10^{-18} \text{ molecules}^{-1} \cdot \text{m}^3 \cdot \text{s}^{-1}$, the peak values of $C_C(\mathbf{u}_{Rx}, t)$ and $C_A(\mathbf{u}_{Rx}, t)$ are approximately identical but the tail of $C_C(\mathbf{u}_{Rx}, t)$ decays faster than the tail of $C_A(\mathbf{u}_{Rx}, t)$. Here, not all type A molecules are converted to type C molecules because there are not enough type B molecules available to react with type A molecules at later times.

In Fig. 7, we study the impact of k_f on $C_C(\mathbf{u}_{Rx}, t)$ for the special setup considered in Subsection III-B, where the concentration of the type B molecules is assumed to be large and thus remains unchanged when reacting with the type A molecules. We further assume $k_b = 0$, $D_A = D_C = 1 \times 10^{-9} \text{ m}^2/\text{s}$, $C_B(\mathbf{u}_{Rx}) = 5 \times 10^{-21} \text{ molecules}/\text{m}^3$, and k_f varies. The dashed lines represent the closed-form expression of $C_C(\mathbf{u}_{Rx}, t)$ in (18). The markers denote $C_C(\mathbf{u}_{Rx}, t)$ obtained with Algorithm 1. The solid lines represent $C_A(\mathbf{u}_{Rx}, t)$ for direct detection. First, we observe that the derived close-form results are in excellent agreement with the results obtained

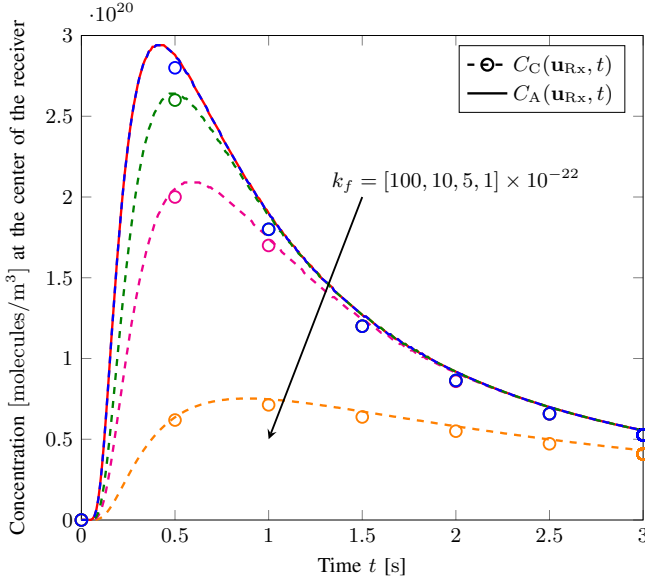


Fig. 7. Concentration of the type A and C molecules at the center of the receiver versus time for direct and indirect detection, respectively, when the concentration of the unrestricted type B molecules is constant. For $C_C(\mathbf{u}_{\text{Rx}}, t)$, the dashed lines and markers denote the closed-form expression in (18) and analysis obtained with Algorithm 1, respectively.

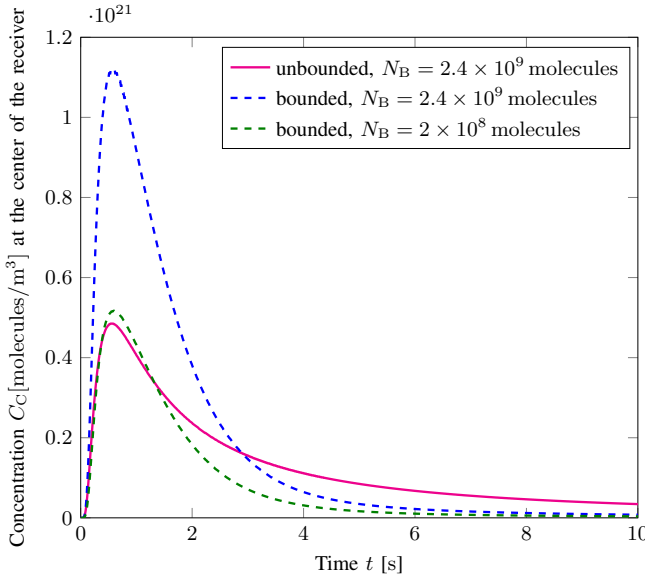


Fig. 8. Concentration of type C molecules at the center of the receiver versus time when type B molecules are released in unbounded and bounded volumes.

by Algorithm 1. We also observe that $C_C(\mathbf{u}_{\text{Rx}}, t)$ approaches $C_A(\mathbf{u}_{\text{Rx}}, t)$ for large k_f , as in Fig. 6. Interestingly, $C_C(\mathbf{u}_{\text{Rx}}, t)$ can be equal to $C_A(\mathbf{u}_{\text{Rx}}, t)$ in Fig. 7 whereas there is a small difference between them in Fig. 6. This is because for the case considered in Fig. 7, $C_B(\mathbf{u}_{\text{Rx}})$ remains constant and all type A molecules can react with type B molecules to create type C molecules.

In Fig. 8, we present the concentrations of the type C molecules at the center of the receiver versus time when the type B molecules are and are not confined to a bounded volume. For the same number of type B molecules released,

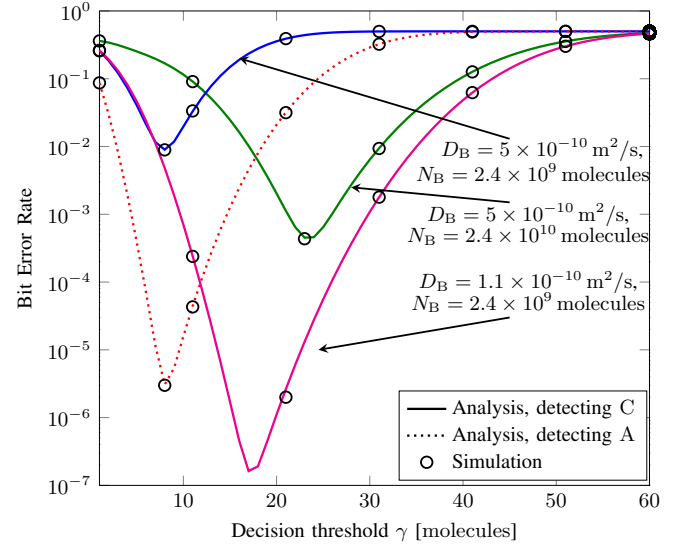


Fig. 9. BER versus decision threshold γ for direct detection via the type A molecules and indirect detection via the type C molecules.

i.e., $N_B = 2.4 \times 10^9$ molecules, the concentration of the type C molecules has a much higher peak value and decreases faster when the type B molecules are restricted to a bounded volume compared to the case when they are not. For a much smaller number of type B molecules, i.e., $N_B = 2 \times 10^8$ molecules, confined to the bounded volume, the same peak value and a faster decrease of C_C can be obtained compared to the case when the type B molecules are in an unbounded volume. Therefore, ISI is less severe when the type B molecules are restricted in a bounded volume. The reason is that, outside the bounded volume, no reaction happens and thus no type C molecules are created which may arrive at the receiver later and contribute to the ISI.

C. System Performance

Fig. 9 depicts the BER of the considered MC system versus decision threshold, γ , for direct and indirect detection. The type B molecules are released at the center of the receiver. We take the ISI caused by the previous two symbols into account, i.e., s_n is interfered by s_{n-1} and s_{n-2} , and the bit interval $T = 10$ s is long enough, such that the contribution of the other previous symbols, e.g., s_{n-3} , to the ISI is negligible. We choose the sampling time t_s equal to the time when $C_C(\mathbf{u}_{\text{Rx}}, t)$ assumes its maximum value, $\max_t C_C(\mathbf{u}_{\text{Rx}}, t)$. From Fig. 9, we observe that the analytical results obtained with (24) and (25) are in excellent agreement with the corresponding Monte-Carlo simulation results. Furthermore, the BER can be reduced significantly by optimizing the decision threshold. We also observe that although $C_C(\mathbf{u}_{\text{Rx}}, t)$ for the case of $D_B = 1.1 \times 10^{-10}$ m²/s and $N_B = 2.4 \times 10^9$ molecules has the highest peak value in Fig. 5, the corresponding optimal decision threshold is smaller than that for the case of $D_B = 5 \times 10^{-10}$ m²/s and $N_B = 2.4 \times 10^{10}$ molecules. This is due to the fact that the optimal threshold depends on both the peak value and the tail of $C_C(\mathbf{u}_{\text{Rx}}, t)$. Moreover, when N_B increases or D_B decreases, the minimum BER value decreases

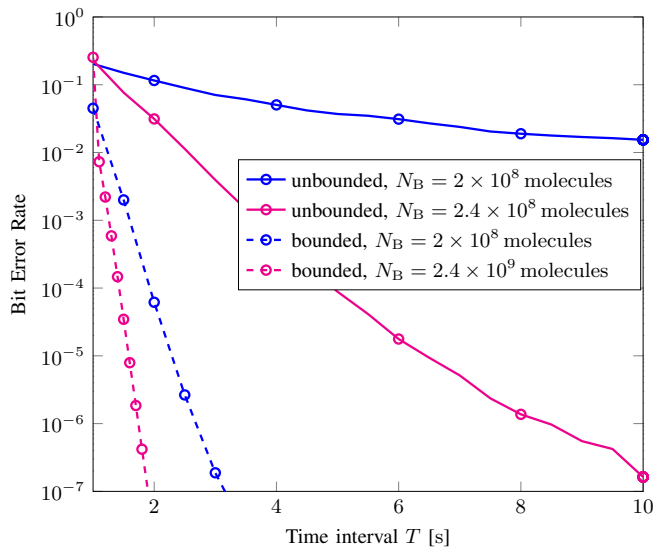


Fig. 10. BER obtained with the optimal decision threshold versus symbol interval T when type B molecules are released in unbounded and bounded volumes.

due to the reduced ISI. When direct detection is not possible, the addition of the type B molecules makes detection via the type C molecules possible even if the resulting BER may be higher compared to the case when direct detection is possible. However, when the released type B molecules are appropriately chosen, e.g., $D_B = 1.1 \times 10^{-10} \text{ m}^2/\text{s}$ and $N_B = 2.4 \times 10^9$ molecules, the proposed indirect detection approach can even achieve a lower BER than direct detection.

Fig. 10 shows the BER obtained with the optimal decision threshold versus the symbol interval length T when the type B molecules are released in unbounded and bounded volumes. As T increases, the impact of ISI reduces and thus the BER decreases. A larger number of released type B molecules results in a lower BER. For the same N_B , the BER with bounded type B molecules is lower than that with unbounded type B molecules because the ISI is less severe as explained in the discussion of Fig. 8. The same BER and a higher data rate, i.e., smaller time intervals, can be achieved with fewer type B molecules released in a bounded volume compared to when their movement is not restricted. This illustrates the efficient use of resources when the type B molecules are restricted to a volume around the receiver.

Fig. 11 presents the BER obtained with the optimal decision threshold versus the number of released type B molecules N_B for different symbol interval lengths T . We observe that for larger T , the BER decreases faster as N_B increases. For the same T , for bounded type B molecules, the BER is lower and decreases faster as N_B increases compared to unbounded type B molecules.

V. CONCLUSIONS

In this work, we proposed a novel detection mechanism for MC systems where the signaling molecules cannot be directly detected at the receiver. Therefore, a molecular probe was introduced to react with the signaling molecules to produce

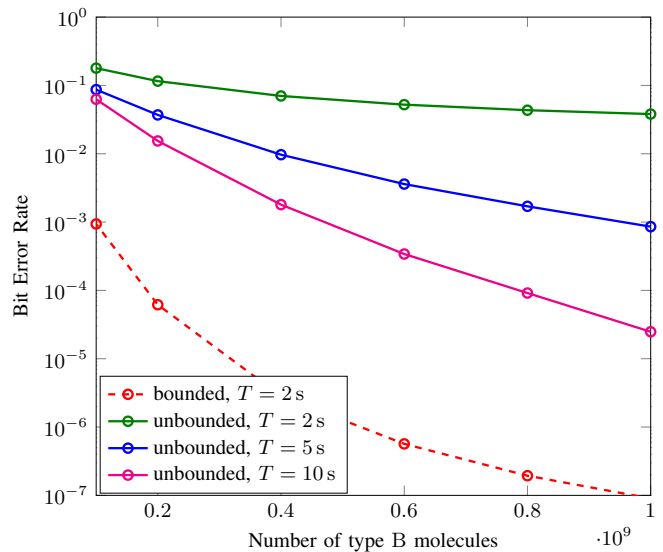


Fig. 11. BER obtained with the optimal decision threshold versus the number of released type B molecules N_B for different symbol interval lengths T .

product molecules that can then be detected at the receiver. The molecular probes needed for the proposed detection mechanism can be deployed differently, i.e., as unrestricted probes and as probes restricted in a small volume around the receiver. For system performance analysis, we developed an efficient iterative algorithm to find the spatio-temporal concentration of the product molecules taking into account diffusion and reactions. For the special case where the probe concentration is constant over time, closed-form expressions for the concentrations were derived. Our results showed that the concentration of the product molecules exhibits a similar characteristic over time as the concentration of the signaling molecules. We analyzed the performance of the MC system using the proposed detection scheme in terms of BER. Our results showed that the BER for indirect detection can be significantly improved by optimizing the decision threshold and can even be lower than the BER for direct detection if the molecular probe is suitably chosen. Moreover, when the molecular probe is kept in a volume around the receiver, the same BER and a higher data rate can be achieved with much fewer molecular probes compared to when the molecular probes are not restricted.

APPENDIX A: PROOF OF COROLLARY 1

We can derive (7) by expanding (6) in cylindrical coordinates with $\tilde{\mathbf{u}} = (\tilde{\rho}, \tilde{\phi}, \tilde{z})$ and substituting

$$\|\mathbf{u} - \tilde{\mathbf{u}}\|^2 = (z - \tilde{z})^2 + \rho^2 + \tilde{\rho}^2 - 2\rho\tilde{\rho}\cos(\tilde{\phi}) \quad (27)$$

into (6). Then, by using

$$\int_{\tilde{\phi}=0}^{2\pi} \exp\left(\frac{2\rho\tilde{\rho}\cos(\tilde{\phi})}{4D_i\Delta t}\right) d\tilde{\phi} = 2\pi I_0\left(\frac{\rho\tilde{\rho}}{2D_i\Delta t}\right), \quad (28)$$

we obtain (7).

APPENDIX B: PROOF OF THEOREM 1

We obtain (9) by following similar steps as in [20, Appendix D] to solve the following set of equations

$$\frac{\partial C_A^{\text{rc}}(\mathbf{u}, t)}{\partial t} = -\kappa_f C_A^{\text{rc}}(\mathbf{u}, t) C_B^{\text{rc}}(\mathbf{u}, t) + \kappa_b C_C^{\text{rc}}(\mathbf{u}, t), \quad (29a)$$

$$\frac{\partial C_B^{\text{rc}}(\mathbf{u}, t)}{\partial t} = -\kappa_f C_A^{\text{rc}}(\mathbf{u}, t) C_B^{\text{rc}}(\mathbf{u}, t) + \kappa_b C_C^{\text{rc}}(\mathbf{u}, t), \quad (29b)$$

$$\frac{\partial C_C^{\text{rc}}(\mathbf{u}, t)}{\partial t} = \kappa_f C_A^{\text{rc}}(\mathbf{u}, t) C_B^{\text{rc}}(\mathbf{u}, t) - \kappa_b C_C^{\text{rc}}(\mathbf{u}, t). \quad (29c)$$

Subtracting (29b) from (29a) and adding (29a) and (29c), respectively, we obtain

$$\frac{\partial (C_A^{\text{rc}}(\mathbf{u}, t) - C_B^{\text{rc}}(\mathbf{u}, t))}{\partial t} = 0, \quad (30)$$

$$\frac{\partial (C_A^{\text{rc}}(\mathbf{u}, t) + C_C^{\text{rc}}(\mathbf{u}, t))}{\partial t} = 0. \quad (31)$$

Equations (30) and (31) have solutions $C_A^{\text{rc}}(\mathbf{u}, t) - C_B^{\text{rc}}(\mathbf{u}, t) = c_{11}(\mathbf{u})$ and $C_A^{\text{rc}}(\mathbf{u}, t) + C_C^{\text{rc}}(\mathbf{u}, t) = c_{12}(\mathbf{u})$, where $c_{11}(\mathbf{u}) = C_A^{\text{rc}}(\mathbf{u}, t_0) - C_B^{\text{rc}}(\mathbf{u}, t_0)$ and $c_{12}(\mathbf{u}) = C_A^{\text{rc}}(\mathbf{u}, t_0) + C_C^{\text{rc}}(\mathbf{u}, t_0)$, respectively. Here, t_0 is the initial time for which the initial conditions are known. Substituting $C_A^{\text{rc}}(\mathbf{u}, t) - C_B^{\text{rc}}(\mathbf{u}, t) = c_{11}(\mathbf{u})$ and $C_A^{\text{rc}}(\mathbf{u}, t) + C_C^{\text{rc}}(\mathbf{u}, t) = c_{12}(\mathbf{u})$ into (29a), we have

$$\begin{aligned} \frac{\partial C_A^{\text{rc}}(\mathbf{u}, t)}{\partial t} = & - \left(\kappa_f (C_A^{\text{rc}}(\mathbf{u}, t))^2 + (-\kappa_f c_{11}(\mathbf{u}) + \kappa_b) \right. \\ & \left. \times C_A^{\text{rc}}(\mathbf{u}, t) - \kappa_b c_{12}(\mathbf{u}) \right), \end{aligned} \quad (32)$$

which can be rewritten as

$$\begin{aligned} & \frac{\partial (C_A^{\text{rc}}(\mathbf{u}, t))}{\kappa_f (C_A^{\text{rc}}(\mathbf{u}, t))^2 + (-\kappa_f c_{11}(\mathbf{u}) + \kappa_b) C_A^{\text{rc}}(\mathbf{u}, t) - \kappa_b c_{12}(\mathbf{u})} \\ & = -\partial t. \end{aligned} \quad (33)$$

Integrating both sides of (33) and using [32]

$$\int \frac{dx}{ax^2 + bx + c} = \frac{1}{\Delta} \log \left(\frac{\Delta - 2ax - b}{\Delta + 2ax + b} \right), \quad (34)$$

where $\Delta = \sqrt{b^2 - 4ac}$, we obtain

$$\begin{aligned} -t + \tilde{c}_4(\mathbf{u}) = & \quad (35) \\ & \frac{1}{c_2(\mathbf{u})} \ln \left(\frac{c_2(\mathbf{u}) - 2\kappa_f C_A^{\text{rc}}(\mathbf{u}, t) + \kappa_f c_{11}(\mathbf{u}) - \kappa_b}{c_2(\mathbf{u}) + 2\kappa_f C_A^{\text{rc}}(\mathbf{u}, t) - \kappa_f c_{11}(\mathbf{u}) + \kappa_b} \right), \end{aligned}$$

where $c_2(\mathbf{u}) = \sqrt{(-\kappa_f c_{11}(\mathbf{u}) + \kappa_b)^2 + 4\kappa_f \kappa_b c_{12}(\mathbf{u})}$ and $\tilde{c}_4(\mathbf{u})$ is a constant with respect to time. Using the initial condition when $t = t_0$ in (35) leads to

$$\tilde{c}_4(\mathbf{u}) = \frac{1}{c_2(\mathbf{u})} \ln \left(\frac{c_2(\mathbf{u}) - \kappa_f c_3(\mathbf{u}) - \kappa_b}{c_2(\mathbf{u}) + \kappa_f c_3(\mathbf{u}) + \kappa_b} \right), \quad (36)$$

where $c_3(\mathbf{u}) = C_A^{\text{rc}}(\mathbf{u}, t_0) + C_B^{\text{rc}}(\mathbf{u}, t_0)$. Defining $c_4(\mathbf{u}) = \exp(c_2(\mathbf{u})\tilde{c}_4(\mathbf{u}))$, substituting (36) into (35), and setting the initial time and the current time, denoted by t_0 and t in this proof, equal to t and $\Delta t + t$, respectively, for each iteration in Algorithm 1, we obtain (9a). Using $C_B^{\text{rc}}(\mathbf{u}, t) = C_A^{\text{rc}}(\mathbf{u}, t) - c_{11}(\mathbf{u})$ and $C_C^{\text{rc}}(\mathbf{u}, t) = c_{12}(\mathbf{u}) - C_A^{\text{rc}}(\mathbf{u}, t)$, it is straightforward to obtain (9b) and (9c), respectively.

APPENDIX C: PROOF OF COROLLARY 3

The expression in (17) is obtained from [14, Eq. (9)] with $k_{-1} = 0$. Adding (2a) and (2c), we obtain

$$\frac{\partial C(\mathbf{u}, t)}{\partial t} = G_A(\mathbf{u}, t) + D_A \nabla^2 C(\mathbf{u}, t), \quad (37)$$

where $C(\mathbf{u}, t) = C_A(\mathbf{u}, t) + C_C(\mathbf{u}, t)$. From the solution $C(\mathbf{u}, t)$ of (37), we obtain (18).

APPENDIX D: PROOF OF COROLLARY 4

As the diffusion and reaction can be decoupled in Δt , to obtain (19), we need to solve the diffusion-only equation

$$\frac{\partial C(\rho, \phi, z, t)}{\partial t} = D \nabla^2 C(\rho, \phi, z, t), \quad (38)$$

for the following initial and boundary conditions

$$C(\rho, \phi, z, t = t_0) = f(\rho, \phi, z), \quad (39)$$

$$\left. \frac{\partial C(\rho, \phi, z, t)}{\partial z} \right|_{z=-\frac{b}{2}, z=\frac{b}{2}} = 0, \quad (40)$$

$$\left. \frac{\partial C(\rho, \phi, z, t)}{\partial \rho} \right|_{\rho=a} = 0. \quad (41)$$

Here, $f(\rho, \phi, z)$ is an arbitrary initial condition at t_0 . Then, we can obtain $C_B^{\text{df}}(\mathbf{u}, t + \Delta t)$ as a function of $C_B^{\text{df}}(\mathbf{u}, t)$ by solving (38) and mapping $C_B^{\text{df}}(\mathbf{u}, t)$ and Δt to the initial condition and t of (38), respectively.

Using variable separation, we assume $C(\rho, \phi, z, t) = P(\rho)\Phi(\phi)Z(z)T(t)$, where $P(\rho)$, $\Phi(\phi)$, $Z(z)$, and $T(t)$ are functions of ρ , ϕ , z , and t , respectively. From (38), we have

$$\begin{aligned} P(\rho)\Phi(\phi)Z(z)T'(t) = & DT \left(\frac{\Phi(\phi)Z(z)}{\rho} \frac{\partial}{\partial \rho} (\rho P'(\rho)) \right. \\ & \left. + \frac{P(\rho)Z(z)}{\rho^2} \Phi''(\phi) + P(\rho)\Phi(\phi)Z''(z) \right), \end{aligned} \quad (42)$$

where $F'(x)$ and $F''(x)$ denote first and second derivative of $F(x)$, respectively. Simplifying (42), we have

$$\begin{aligned} T'(t) = & DT \left(\frac{1}{\rho P(\rho)} (P'(\rho) + \rho P''(\rho)) \right. \\ & \left. + \frac{1}{\Phi(\phi)\rho^2} \Phi''(\phi) + \frac{Z''(z)}{Z(z)} \right) \end{aligned} \quad (43)$$

\Leftrightarrow

$$\begin{aligned} \frac{1}{\rho P(\rho)} (P'(\rho) + \rho P''(\rho)) + \frac{1}{\Phi(\phi)\rho^2} \Phi''(\phi) + \frac{Z''(z)}{Z(z)} \\ - \frac{T'(t)}{DT(t)} = 0 \end{aligned} \quad (44)$$

\Leftrightarrow

$$\frac{1}{\rho P(\rho)} (P'(\rho) + \rho P''(\rho)) + l^2 = 0, \quad (45a)$$

$$\frac{1}{\Phi(\phi)\rho^2} \Phi''(\phi) = 0, \quad (45b)$$

$$\frac{Z''(z)}{Z(z)} = k^2, \quad (45c)$$

$$-\frac{T'(t)}{DT(t)} = h^2, \quad (45d)$$

$$k^2 + h^2 = l^2. \quad (45e)$$

Eq. (45b) is obtained due to the fact that the system is symmetric and the concentration does not depend on ϕ , i.e., $\Phi(\phi)$ is a constant. The solution of (45c) for initial condition (40) is $Z(z) = A \cos(\sqrt{-k^2}z) = A \cos\left(\frac{n\pi}{b}z\right)$, where $-k^2 = \frac{n^2\pi^2}{b^2}$, $n = 0, 1, 2, 3, \dots$, and A is a constant. The solution of (45a) for initial condition (41) is $P(\rho) = J_0\left(\frac{l_j}{a}\rho\right)$, where l_j satisfies $J_0'(l_j) = 0$ and $j = 0, 1, 2, 3, \dots$. Then, due to (45e), the solution of (45d) is $T(t) = Ce^{-h^2Dt} = Ce^{\left(-\frac{n^2\pi^2}{b^2} - \frac{l_j^2}{a^2}\right)Dt}$, where C is a constant. Hence, we have

$$C(\rho, \phi, z, t) = \sum_{n=0}^{\infty} \sum_{j=0}^{\infty} a_{nj} J_0\left(\frac{l_j}{a}\rho\right) \cos\left(\frac{n\pi z}{b}\right) e^{\left(-\frac{n^2\pi^2}{b^2} - \frac{l_j^2}{a^2}\right)Dt}, \quad (46)$$

where a_{nj} is a constant. From (39), we have

$$\sum_{n=0}^{\infty} \sum_{j=0}^{\infty} a_{nj} J_0\left(\frac{l_j}{a}\rho\right) \cos\left(\frac{n\pi z}{b}\right) = f(\rho, \phi, z). \quad (47)$$

To find a_{nj} , we multiply each side of (47) by $J_0\left(\frac{l_j}{a}\rho\right) \cos\left(\frac{n\pi z}{b}\right)$, taking integrals with respect to ρ and z , respectively, and use the following orthogonality relations [33]

$$\int_0^a J_0\left(\frac{l_j}{a}\rho\right) J_0\left(\frac{l_{\tilde{j}}}{a}\rho\right) \rho d\rho = \begin{cases} \frac{a^2}{2}, & \text{for } j = \tilde{j} = 0 \\ \frac{a^2 J_0^2(l_j)}{2} \delta_{j\tilde{j}}, & \text{for } j, \tilde{j} > 0 \end{cases} \quad (48)$$

$$\int_{-\frac{b}{2}}^{\frac{b}{2}} \cos\left(\frac{n\pi}{b}z\right) \cos\left(\frac{\tilde{n}\pi}{b}z\right) dz = \begin{cases} b, & \text{for } n = \tilde{n} = 0 \\ \frac{b}{2} \delta_{n\tilde{n}}, & \text{for } n, \tilde{n} > 0 \end{cases} \quad (49)$$

where $\delta_{x\tilde{x}} = 1$ when $x = \tilde{x}$ and $\delta_{x\tilde{x}} = 0$ when $x \neq \tilde{x}$. Then, changing the variables of the integrals, i.e., $\rho \rightarrow \tilde{\rho}$, $\phi \rightarrow \tilde{\phi}$, and $z \rightarrow \tilde{z}$, we obtain

$$a_{00} = \int_{-\frac{b}{2}}^{\frac{b}{2}} \int_0^a \frac{2}{a^2 b} \tilde{\rho} f(\tilde{\rho}, \tilde{\phi}, \tilde{z}) d\tilde{\rho} d\tilde{z}, \quad (50)$$

$$a_{0j} = \int_{-\frac{b}{2}}^{\frac{b}{2}} \int_0^a \frac{2}{a^2 J_0^2(l_j) b} J_0\left(\frac{l_j}{a}\tilde{\rho}\right) \tilde{\rho} f(\tilde{\rho}, \tilde{\phi}, \tilde{z}) d\tilde{\rho} d\tilde{z}, \quad (51)$$

$$a_{n0} = \int_{-\frac{b}{2}}^{\frac{b}{2}} \int_0^a \frac{4}{a^2 b} \cos\left(\frac{n\pi}{b}\tilde{z}\right) \tilde{\rho} f(\tilde{\rho}, \tilde{\phi}, \tilde{z}) d\tilde{\rho} d\tilde{z}, \quad (52)$$

$$a_{nj} = \int_{-\frac{b}{2}}^{\frac{b}{2}} \int_0^a \frac{4}{a^2 J_0^2(l_j) b} \cos\left(\frac{n\pi}{b}\tilde{z}\right) J_0\left(\frac{l_j}{a}\tilde{\rho}\right) \tilde{\rho} f(\tilde{\rho}, \tilde{\phi}, \tilde{z}) d\tilde{\rho} d\tilde{z}. \quad (53)$$

Substituting (50), (51), (52), and (53) into (46) and setting $t_0 = t$ and t in this proof equal to Δt , we obtain (19).

REFERENCES

- [1] T. N. Cao, V. Jamali, W. Wicke, P. L. Yeoh, N. Zlatanov, J. Evans, and R. Schober, "Chemical reactions-based detection mechanism for molecular communications," in *Proc. IEEE Wireless Commun. Netw. Conf.*, June 2020, pp. 1–7.
- [2] V. Jamali, A. Ahmadzadeh, W. Wicke, A. Noel, and R. Schober, "Channel modeling for diffusive molecular communication—A tutorial review," *Proceedings of the IEEE*, vol. 107, no. 7, pp. 1256–1301, July 2019.
- [3] D. Bi, A. Almpanis, A. Noel, Y. Deng, and R. Schober, "A survey of molecular communication in cell biology: Establishing a new hierarchy for interdisciplinary applications," *IEEE Commun. Surveys Tuts.*, vol. 23, no. 3, pp. 1494–1545, 2021.
- [4] W. Pan, X. Chen, X. Yang, N. Zhao, L. Meng, and F. H. Shah, "A molecular communication platform based on body area nanonetwork," *Nanomaterials*, vol. 12, no. 4, Feb. 2022.
- [5] A. D. Johnson, R. M. Curtis, and K. J. Wallace, "Low molecular weight fluorescent probes (LMFPs) to detect the group 12 metal triad," *Chemosensors*, vol. 7, no. 2, Apr. 2019.
- [6] W. Wicke, H. Unterweger, J. Kirchner, L. Brand, A. Ahmadzadeh, D. Ahmed, V. Jamali, C. Alexiou, G. Fischer, and R. Schober, "Experimental system for molecular communication in pipe flow with magnetic nanoparticles," *IEEE Trans. Mol. Biol. Multi-Scale Commun.*, Early Access, 2021.
- [7] N. Farsad, W. Guo, and A. W. Eckford, "Tabletop molecular communication: Text messages through chemical signals," *PLOS ONE*, vol. 8, no. 12, p. e82935, Dec. 2013.
- [8] M. Natali, L. Soldi, and S. Giordani, "A photoswitchable Zn(II) selective spiropyran-based sensor," *Tetrahedron*, vol. 66, no. 38, pp. 7612–7617, Sep. 2010.
- [9] W. Luo, M. Liu, T. Yang, X. Yang, Y. Wang, and H. Xiang, "Fluorescent ZnII chemosensor mediated by a 1,8-Naphthyridine derivative and its photophysical properties," *Chem. Open*, vol. 7, no. 8, pp. 639–644, Aug. 2018.
- [10] L. Zhao, L. Zhao, Y. Miao, C. Liu, and C. Zhang, "Construction of a turn off-on-off fluorescent system based on competitive coordination of Cu(2+) between 6,7-dihydroxycoumarin and pyrophosphate ion for sensitive assay of pyrophosphatase activity," *J. Anal. Methods Chem.*, p. 4306838, Sep. 2016.
- [11] X. Liu, P. Wang, J. Fu, K. Yao, K. Xue, and K. Xu, "Turn-on fluorescent sensor for Zinc and Cadmium ions based on quinolone and its sequential response to phosphate," *J. Luminescence*, vol. 186, pp. 16–22, June 2017.
- [12] D. Bi, Y. Deng, M. Pierobon, and A. Nallanathan, "Chemical reactions-based microfluidic transmitter and receiver design for molecular communication," *IEEE Trans. Commun.*, vol. 68, no. 9, pp. 5590–5605, Sep. 2020.
- [13] U. A. K. Chude-Onkonkwo, R. Malekian, and B. T. S. Maharaj, "Molecular communication model for targeted drug delivery in multiple disease sites with diversely expressed enzymes," *IEEE Trans. Nanobiosci.*, vol. 15, no. 3, pp. 230–245, Apr. 2016.
- [14] A. Noel, K. Cheung, and R. Schober, "Improving receiver performance of diffusive molecular communication with enzymes," *IEEE Trans. Nanobiosci.*, vol. 13, no. 1, pp. 31–43, Mar. 2014.
- [15] Y. Cho, B. Yilmaz, W. Guo, and C. Chae, "Effective inter-symbol interference mitigation with a limited amount of enzymes in molecular communications," *Trans. Emerging Telecommun. Technol.*, vol. 28, no. 7, p. e3106, July 2017.
- [16] H. Arjmandi, M. Zoofaghari, and A. Noel, "Diffusive molecular communication in a biological spherical environment with partially absorbing boundary," *IEEE Trans. Commun.*, vol. 67, no. 10, pp. 6858–6867, Oct. 2019.
- [17] C. T. Chou, "Extended master equation models for molecular communication networks," *IEEE Trans. Nanobiosci.*, vol. 12, no. 2, pp. 79–92, June 2013.
- [18] X. Huang, Y. Fang, A. Noel, and N. Yang, "Membrane fusion-based transmitter design for static and diffusive mobile molecular communication systems," *IEEE Trans. Commun.*, vol. 70, no. 1, pp. 132–148, Jan. 2022.
- [19] M. Farahnak-Ghazani, G. Aminian, M. Mirmohseni, A. Gohari, and M. Nasiri-Kenari, "On medium chemical reaction in diffusion-based molecular communication: A two-way relaying example," *IEEE Trans. Commun.*, vol. 67, no. 2, pp. 1117–1132, Feb. 2019.
- [20] V. Jamali, N. Farsad, R. Schober, and A. Goldsmith, "Diffusive molecular communications with reactive molecules: Channel modeling and signal design," *IEEE Trans. Mol. Biol. Multi-Scale Commun.*, vol. 4, no. 3, pp. 171–188, Sep. 2018.
- [21] H. Abin, A. Gohari, and M. Nasiri-Kenari, "An analytical model for molecular communication over a non-linear reaction-diffusion medium," *IEEE Trans. Commun.*, vol. 69, no. 12, pp. 8042–8054, Dec. 2021.
- [22] L. Zha, Y. Deng, A. Noel, M. Elakashan, and A. Nallanathan, "Transceiver observations in asymmetric and symmetric diffusive molecular communication systems," in *Proc. IEEE Global Commun. Conf.*, Abu Dhabi, United Arab Emirates, Dec. 2018, pp. 206–212.
- [23] C. Ronco, R. Bellomo, J. A. Kellum, and Z. Ricci, "Chapter 139 - principles of extracorporeal circulation and transport phenomena," in *Critical Care Nephrology*. Philadelphia, USA: Elsevier, 2019.

- [24] B. Alberts, A. Johnson, J. Lewis, M. Raff, K. Roberts, and P. Walter, *Molecular Biology of the Cell*. New York, NY, USA: Garland Science, 2015.
- [25] K. Li, *Ceramic Membranes for Separation and Reaction*. West Sussex, England: John Wiley & Sons, Ltd, 2007.
- [26] G. Hermanson, *Bioconjugate Techniques*. New York, NY, USA: Academic, 2008.
- [27] M. Vicente and J. Löwe, "Ring, helix, sphere and cylinder: the basic geometry of prokaryotic cell division," *EMBO Rep.*, vol. 4, no. 7, p. 655–660, July 2003.
- [28] K. D. Young, "Bacterial morphology: Why have different shapes?" *Curr Opin Microbiol.*, vol. 10, no. 6, p. 596–600, Dec. 2007.
- [29] R. Chang, *Physical Chemistry for the Biosciences*. Mill Valley, CA, USA: University Science, 2005.
- [30] L. Debnath, *Nonlinear Partial Differential Equations for Scientists and Engineers*. New York, USA: Springer, 2011.
- [31] V. Jamali, A. Ahmadzadeh, and R. Schober, "On the design of matched filters for molecule counting receivers," *IEEE Commun. Lett.*, vol. 21, no. 8, pp. 1711–1714, Aug. 2017.
- [32] I. S. Gradshteyn and I. M. Ryzhik, *Table of Integrals, Series, and Products*. Boston, MA, USA: Academic, 2007.
- [33] J. Lambers, "Math 415/515," Lecture Notes, Fall 2013-2014, [Online]. Available: <https://www.math.usm.edu/lambers/mat415/lecture15.pdf>.